USE OF TOPOGRAPHY IN THE CONTEXT OF THE GOCE SATELLITE MISSION – SOME EXAMPLES

Moritz Rexer[(1)], Christian Hirt[(1,2)], Sten Claessens[(2)], Carla Braitenberg[(3)]

[(1)]*Institut für Astronomische und Physikalische Geodäsie & Institute for Advanced Study, Technische Universität München, Arcisstr. 21, D-80333 München (Germany), Email: m.rexer@tum.de*
[(2)]*Department of Spatial Sciences, Curtin University, GPO Box U1987, Perth, WA 6845 (Australia), Email: c.hirt@curtin.edu.au, s.claessens@curtin.edu.au*
[(3)]*Dipartimento di Matematica e Geoscienze, Universita´degli Studi di Trieste, via Weiss 1, Palazzina C, 34127 Trieste (Italy), Email: berg@units.it*

ABSTRACT

The uppermost masses of the lithosphere - notably the land topography, bathymetry and ice - make a significant contribution to the gravity signal captured by ESA's GOCE gravity mission [1,2]. This circumstance is used 1) to evaluate ESA GOCE gravity field models of all generations, 2) to evaluate various topographic data sets and 3) to compute a global Bouguer gravity anomaly map. All of the above is facilitated through forward modelling of the ellipsoidal topographic potential (ETP) applying the *Harmonic Combination Method* [3]. Curtin University's new rock-equivalent topography (RET) model, taken from the Earth2014 suite of topographic data [4], serves as topographic input model for the gravity forward modelling. ESA GOCE models show steady improvement over time and prove to be sensitive for topographic gravity signals at scales of ~100 km and finer. Using the release-5 GOCE models as a reference, Curtin University's RET models are found to improve over time too. Finally, we demonstrate that the spectral representation of the ETP allows straightforward computation of global Bouguer anomaly maps.

1. INTRODUCTION

Newton's law of gravitation describes the universal relationship between the mass elements of a body and the generated gravitational potential. In other words it allows (mostly under certain simplifying assumptions) the computation of Earth's topographic potential $\bar{V}^T$. The topographic potential may be interpreted as prediction of Earth's true gravitational potential $\bar{V}$ as, e.g., sensed by ESA's (European Space Agency) Earth Explorer satellite mission GOCE (Gravity field and steady-state Ocean Circulation Explorer) [1]. Especially short and local-scale gravity signals are strongly dominated by the gravity contributions of the topographic masses [1]. The global availability of accurate high-resolution digital elevation data sets [4, 5] allows forward modelling of the topographic potential from the topographic masses [3,6,7], providing readily usable solutions to Newton's integral law, and triggering a range of applications related to ESA's high-resolution (purely observation-based) GOCE gravity field models [8].

Most importantly, modern gravity field modelling often uses GOCE gravity data as starting point (usually combined with other satellite observation data and/or terrestrial data) together with forward modelled gravity. The latter is meant to either fill no-data areas (e.g. EGM2008 [9]) or to augment gravity field models beyond the resolution of available terrestrial observations (e.g. GGMplus [10]), which is conceptually very similar. Another wide field of applications relies on the difference between observed gravity taken from GOCE gravity field models g_{GOCE} and predicted (=forward-modelled) topographic gravity g_{TOPO} :

$$dg = g_{GOCE} - g_{TOPO}, \qquad (1)$$

where dg denotes the residual gravity defined for a point P on or outside of the topographic masses. This work provides three examples of applications for Eq. (1).

- First, the gravity differences can be used as a quality indicator for GOCE gravity field models (or any other geopotential model), as they allow quantification of how good the agreement between the represented gravity and the (predicted) topography-implied gravity is. This has already been done for ESA GOCE models up to the third generation [2]. It was also shown that GOCE delivers improvements of gravity field knowledge over the Himalayas, Africa, the Andes and other remote areas. Here we will investigate the sensitivity of all ESA GOCE models regarding topography-implied gravity with updated topographic information and an improved forward-modelling technique: the *Harmonic Combination Method* [3]. The spectral method rigorously provides the ellipsoidal topographic potential compatible to ESA GOCE models.

- Second, we can reverse the above strategy and use the residual gravity dg to evaluate a) the quality of the topographic data being used as input for the forward modelling and b) the forward modelling technique as such. In this case one of the latest GOCE gravity field models serves as a reference to assess topographic gravity data sets. In [12] it could be shown that the topographic information in the bedrock model Bedmap2 improved with respect to the predecessor

model Bedmap 1 over Antarctica, with the help of GOCE data. Using this concept, we here evaluate five different global topography models and investigate underlying forward-modelling techniques and concepts.

- Third, the residual gravity dg from Eq. (1) may be used to locate mass irregularities in the topography and the planets interior. The mass irregularities are often described using the concept of Bouguer gravity anomalies. Bouguer anomalies can be used for geophysical inversions and to retrieve parameters such as rock-density or crustal thickness of planetary bodies [16]. The Bouguer anomaly in classical (geodetic) definition uses the local topography in planar approximation [11]. With the topographic potential in spectral form, the global topographic masses and ellipsoidal shape of the Earth are accounted for in our study. As such our Bouguer anomalies improve conceptionally over planar ones (see section 3.4). We show that the creation of a global map of Bouguer anomalies – in modern definition – is straightforward using the new GOCE fields and spectral forward modelling.

The data sets used in our study are described in section 2. In section 3.1 we explain the methodology implied in the forward-modelling of the topographic masses. The indicators used for the evaluation of ESA GOCE models and topographic information are given in section 3.2 and 3.3. The computation of Bouguer anomalies in this work is explained in section 3.4. Finally, section 4 presents all the results and in section 5 conclusions are given together with an outlook on future work.

2. DATA

2.1 GOCE gravity field models

A multitude of GOCE-based gravity field models have been produced since the satellite's gravity gradient data became available [8] in late 2009. Most important models among them are ESA's High-Level Processing (HPF) facilities' official model releases, which are following three different modelling approaches: the direct-method (DIR) [13], the space-wise method (SPW) [14] and the time-wise method (TIM) [15]. In mid-2014 the fifth release of the models was made available (SPW models only exist up to third generation), covering gravity data of the whole period of GOCE's in-orbit operational phase.

This work will focus on the models of the DIR and TIM approach, all listed chronologically in Tab. 1. While the TIM models rely on GOCE data solely and thus represent an important independent source for validation of other gravity data, DIR models have been designed to optimally use all available present-day satellite gravity data in order to yield excellent performance over the entire spectrum. GOCE data has therefore been combined

with GRACE (Gravity Recovery And Climate Change Experiment). satellite gravity data.

	Release Date	Model Acronym	Data Period
R1	2010	DIR1	2009/11/1 - 2010/01/11
		TIM1	2009/11/1 - 2010/01/11
R2	2011	DIR2	2009/11/1 - 2010/06/30
		TIM2	2009/11/1 - 2010/07/05
R3	2011	DIR3	2009/11/1 - 2011/04/19
		TIM3	2009/11/1 - 2011/04/17
R4	2013	DIR4	2009/11/1 - 2012/08/01
		TIM4	2009/11/1 - 2012/06/19
R5	2014	DIR5	2009/11/1 - 2013/10/20
		TIM5	2009/11/1 - 2013/10/20

Table 1 : GOCE models and data periods; DIR(1,2,3,4,5): GO_CONS_GCF_2_DIR(1,2,3,4,5); TIM(1,2,3,4,5): GOC_CONS_GCF_2_TIM(1,2,3,4,5)

2.2 Topography

Topography as needed as an input for the forward modelling of the topographic potential has been taken from the Earth2014 topographic suite, created at Curtin University [4]. Earth2014 comprises (amongst others) a rock-equivalent topography (RET) model at 1 arc min resolution, which is based on the latest freely available topographic data. The sources for the elevations in Earth2014 are: SRTM v4.1 in continental regions, SRTM30_PLUS v9 bathymetry over the oceans, Bedmap2 over Antarctica and GBT v3 over Greenland. Following the concept of RET, the model provides elevations equivalent to a uniform rock mass-density. Thereby, layers of oceans, major inland water bodies, ice-sheets, ice-shelves and water below ice are compressed to layers of a thickness that would equal their mass using rock mass-density (here 2670 kg/m³). For further information on the creation of the model we refer to the detailed description in [4]. Earth2014 topography data sets are superior to previous ones (e.g., Earth2012 or ETOPO1) and the mass modelling is more complete compared to the predecessor models RET2012 [3] and RET2011 [2] (see also section 4.2).

3. METHODS

3.1 Forward modelling of the potential of the topographic masses

For the forward modelling of the ellipsoidal topographic potential we make use of the *Harmonic Combination Method* (HCM) [3]. The HCM uses rock-equivalent topography as input and generates the ellipsoidal topographic potential from a binominal series combining surface spherical harmonic coefficients of different powers of the RET model elevations. The outcome of the HCM are fully normalised solid spherical coefficients of the topographic potential (short: topopotential) in
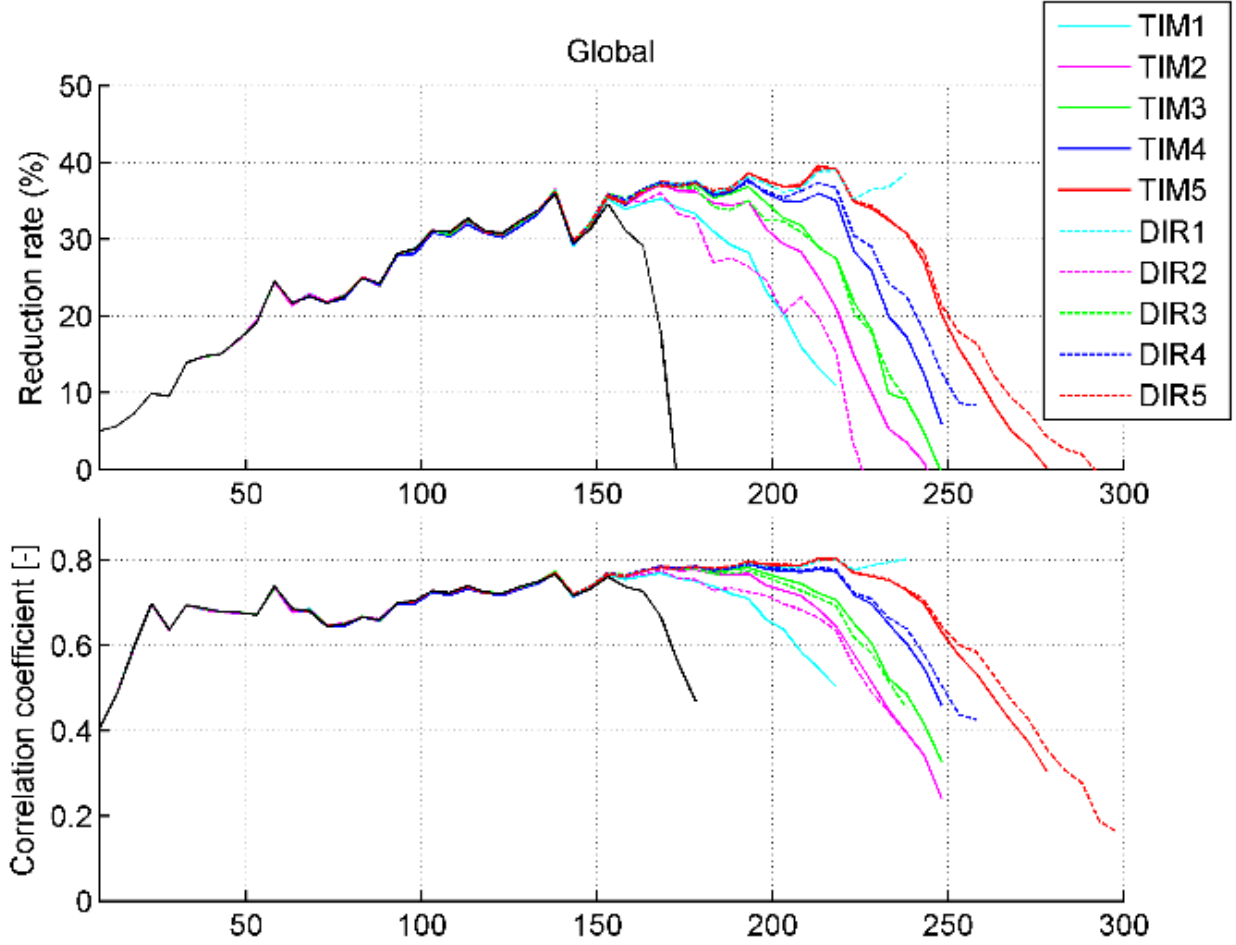
Figure 1 : Evaluation of 5 generations of ESA GOCE models from the time-wise method (TIM: solid lines) and the direct method (DIR: dashed lines) using the topographic potential model dV_ELL_RET2014. Black ITG-GRACE2010S.

ellipsoidal approximation $\bar{V}_{nm}^{R,T}$, which are compatible to ESA GOCE models (and other GGMs), in that, Earth's ellipsoidal shape is accounted for in the mass modelling. The computation of $\bar{V}_{nm}^{R,T}$ relies on

$$\bar{V}_{nm}^{R,T} = \frac{4\pi\rho b^3}{M(2n+1)(n+3)} \left(\frac{b}{R}\right)^n$$ (2)

$$\sum_{k=1}^{n+3} \binom{n+3}{k} \sum_{j=0}^{\infty}(-1)^j \binom{-\frac{n+3}{2}}{j} e^{2j} \; (contin.)$$

$$\sum_{i=-j}^{j} \bar{K}_{nm}^{2i,2j} \, \bar{d}_{n+2i,m}^{(k)}, \; (contin.)$$

where $\bar{d}_{n+2i,m}^{(k)}$ denote the fully normalised surface spherical harmonic coefficients of the RET to the power of k, following

$$\bar{d}_{nm}^{(k)} = \frac{1}{4\pi} \int_\sigma \left(\frac{H^{RET}}{r_e}\right)^k \bar{Y}_{nm} d\sigma$$ (3)

with ρ being the density (used in the RET model), M the Earth's mass, R the potential model's reference radius, r_e the ellipsoidal radius, $\bar{K}_{nm}$ the fully normalized sinusoidal Legendre weight functions [18], H^{RET} the

height extracted from the RET model and $\bar{Y}_{nm}$ the fully normalized spherical harmonic functions. The parameters b and e^2 are the semi-minor axis and the first numerical eccentricity of the underlying reference ellipsoid, respectively. Convergence of the binominal series is reached already for $k_{max} = 7$ and $j_{max} = 30$ (for expansions up to degree 2190), cf. [3]. Similar to EGM2008 [9] an additional 'tail' of spherical harmonic coefficients reflects the ellipsoidal approximation level. It is thus recommended to use all coefficients of an ETP model created by the HCM if the full resolution is sought. For high degrees, say >1000, truncation of the series may lead to serious error patterns of increasing nature towards the poles, reaching amplitudes in the order of ~100 mGal. However, this effect is below the mGal-level for the harmonic degrees investigated here. Isostatic compensation of masses is currently not accounted for in the modelling. A full account of the HCM is given in [3].

3.2 Reduction rates

Reduction rates (RRs) quantify the extent to which gravity generated by the topography is contained in a GOCE gravity field model (see section 2.1). They are defined (e.g.) in [2] as
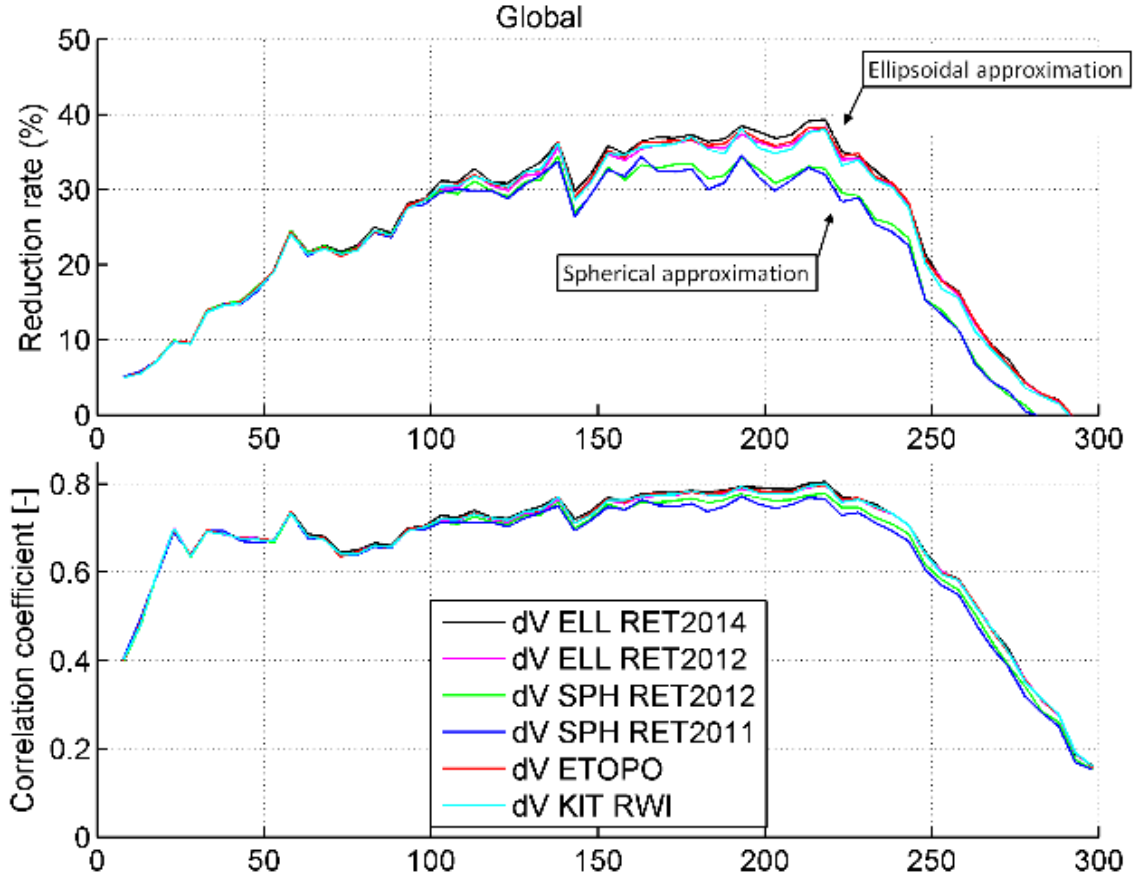
Figure 2 : Evaluation of different topographic data sets and their respective topographic potential models w.r.t. the model GO_CONS_GCF_DIR5 in terms of reduction rates (upper plot) and correlation coefficients (lower plot).

$$RR = 100\% \left(1 - \frac{RMS(\delta g_{TOPO} - \delta g_{GOCE})}{RMS(\delta g_{TOPO})}\right) \qquad (4)$$

where RMS denotes root-mean-square, δg_{TOPO} denote a grid of gravity disturbances expanded from a model of the topographic potential and δg_{GOCE} denote a grid of gravity disturbances expanded from one of GOCE gravity field models. Values close to zero indicate no topographic signal is contained in the respective GOCE model. The authors in [2] find that RR values of 30% to 40% already indicate that topographic gravity signal is well represented in the model.

3.3 Correlation Coefficients

Correlation Coefficients (CCs) are another means to judge the relation between the predicted topographic gravity signal and the observed gravitational signal. They shall quantify the general agreement between the gridded functional given by (1) the GOCE gravity field model and (2) the topopotential. They are defined as (see [12])

$$CC = \frac{\sum(\delta g_{GOCE} - \overline{\delta g_{GOCE}})\sum(\delta g_{TOPO} - \overline{\delta g_{TOPO}})}{\sqrt{\sum(\delta g_{GOCE} - \overline{\delta g_{GOCE}})^2 \sum(\delta g_{TOPO} - \overline{\delta g_{TOPO}})^2}} \qquad (5)$$

where the bar over the parameter denotes the mean value. CCs range between 0 and 1, where very good agreement between two functions is indicated by values of about 0.7 to 0.9 [2]. As CCs and RRs are defined in the space domain, they can either be computed globally, or for an arbitrary region of interest.

3.4 Computation of Bouguer anomalies

Bouguer anomalies Δg_B are computed through spherical harmonic synthesis (SHS) using a model of the topographic potential and a GOCE gravity field model (see section 2.1) given by

$$\Delta g_B(P) = \delta g_{GOCE}(P) - \delta g_{TOPO}(P), \qquad (6)$$

where P is the common computation point. P needs to be located on or outside of the topographic masses, as gravity inside the masses cannot be correctly extracted from the models (the gravitational field is only harmonic outside the gravitational body). For reasons of convenience, an evaluation height of 10 km has been chosen for the computation of global Bouguer anomaly

maps in section 4.3, to be entirely outside of Earth's masses.

Alternatively, prior the SHS, spherical harmonic Bouguer coefficients $\bar{B}_{nm}^R$ may be computed by

$$\bar{B}_{nm}^R = \bar{V}_{nm}^R - \bar{V}_{nm}^{R,T}. \tag{7}$$

in this case Bouguer anomalies (in terms of gravity disturbances) may be synthesised directly from the $\bar{B}_{nm}^R$ coefficients at P. Application of Eq. (7) requires that the defining constants GM and a of the GOCE models and those used in the forward modelling (2) are the same. Note that this kind of gravity anomaly does not follow the classical planar (geodetic) definition of Bouguer anomalies. Rather, it is a modern form of Bouguer gravity anomalies and similar to those often used in planetary sciences (see e.g. [16]) and quite similar to the spherical Bouguer gravity anomalies on Earth defined in [6].

4. RESULTS

4.1 Evaluation of ESA GOCE gravity field models using the Topographic Potential

For the evaluation of ESA GOCE models we take the ellipsoidal topographic potential model dV_ELL_RET2014 as a reference, which is generated by the HCM (section 3.1) applied to Earth2014's RET model (section 2.2).

The spectral representation of both models enables an investigation of the agreement between GOCE gravity and predicted (topographic) gravity in narrow spectral bands using the concept of CCs and RRs. A spectral resolution of five degrees has been chosen in this work.

Figure 1 depicts the globally calculated RRs and CCs by spherical harmonic degree. The different models' curves start to diverge near degree 150, where the noise level of the each model becomes apparent (below degree 150 they largely coincide). both from the RRs and the CCs, an overall (global) improvement over all GOCE model generations can be observed over time, as the curves drop at higher degrees with each release. The only exception is the DIR1 model, which contains terrestrial information at short scales [2] and therefore is not comparable. Highest RRs of almost 40 % are being observed for DIR5 and TIM5 between degree 210 and 220, and CCs reach a value of 0.8 (DIR5 and TIM5 between degree 210 and 220). Looking at the final GOCE models of both methods, DIR5 clearly has a better agreement with topography-implied topography signal in the very short scales (beyond degree 250). Zero reduction of signal strengths seems to be reached near degree 280 for TIM5 and near 290 for DIR5. Although only marginal (and barely visible in Fig.1) it shall be noted that both 5$^{\text{th}}$ generation models do exhibit lower CCs and RRs than some of their predecessor models in the spectral band 150 to 190.

4.2 Reversal: Evaluation of topographic data using ESA GOCE gravity field models

In reverse manner to the previous section, we may use RRs and CCs to evaluate different topographic potential models and their underlying topographic data sets. In addition to Curtin's RET models (dV_SPH_RET2011, dV_SPH_RET2012 and dV_ELL_RET2014; see section 2.2 and 3.1) the models dV_ETOPO and dV_KIT_RWI are evaluated: dV_ETOPO relies on a RET variant of ETOPO1 and the HCM; dV_KIT_RWI are topographic potential coefficients of the Rock-Water-Ice (RWI) model of the Karlsruhe Institute of Technology (KIT) that (opposite to the RET models) were generated in the space domain through numerical integration over mass prisms (without condensation) and subsequent spherical harmonic analysis (SHA), [19].

Taking GO_CONS_GCF_DIR5 as a reference, the RRs and CCs for the various topographic potential models (Fig. 2) exhibit that the topopotential model dV_ELL_RET2014 (black line) is the best prediction of (observed) GOCE gravity. DIR5 gravity amplitudes are best reduced almost over the entire spectrum by this topopotential model (especially in the spectral band 170 … 230), reaching a maximum of 39 % reduction near degree 220. In general, the curves start to diverge near degree 100; below degree 100 the curves largely coincide. A clear distinction between topopotential in spherical approximation (dV_SPH_RET2011: blue line, dV_SPH_RET2012: green line) and ellipsoidal approximation (other models) becomes visible. The latter gives higher RRs and CCs because DIR5 (similar to all other GOCE models) is in ellipsoidal approximation, too. Higher RRs and CCs in dV_ELL_RET2014 compared to dV_ELL_RET2012 may be explained by 1) improved topographic information in the RET2014 model (Bedmap2 instead of Bedmap1, GBT_V3 instead of GLOBE) and 2) improved RET modelling (the latest version also accounts for ice-shelves and water below ice). The ellipsoidal potential model dV_ETOPO (red line) shows lower RRs and CC values than dV_ELL_RET2014 (though it is closest) which justifies the creation of Earth2014 [4]: a topographic models suite that incorporates the most recent topographic mass models. The fact that the RET models show largely similar performance compared to the ellipsoidal topographic potential model dV_KIT_RWI which was computed by a more sophisticated modelling approach (masses are taken into account at their actual location, whereas ice/water masses in RET models are compressed) may provide evidence that errors associated with the concept of rock-equivalent topography do not so much play a role in this study.
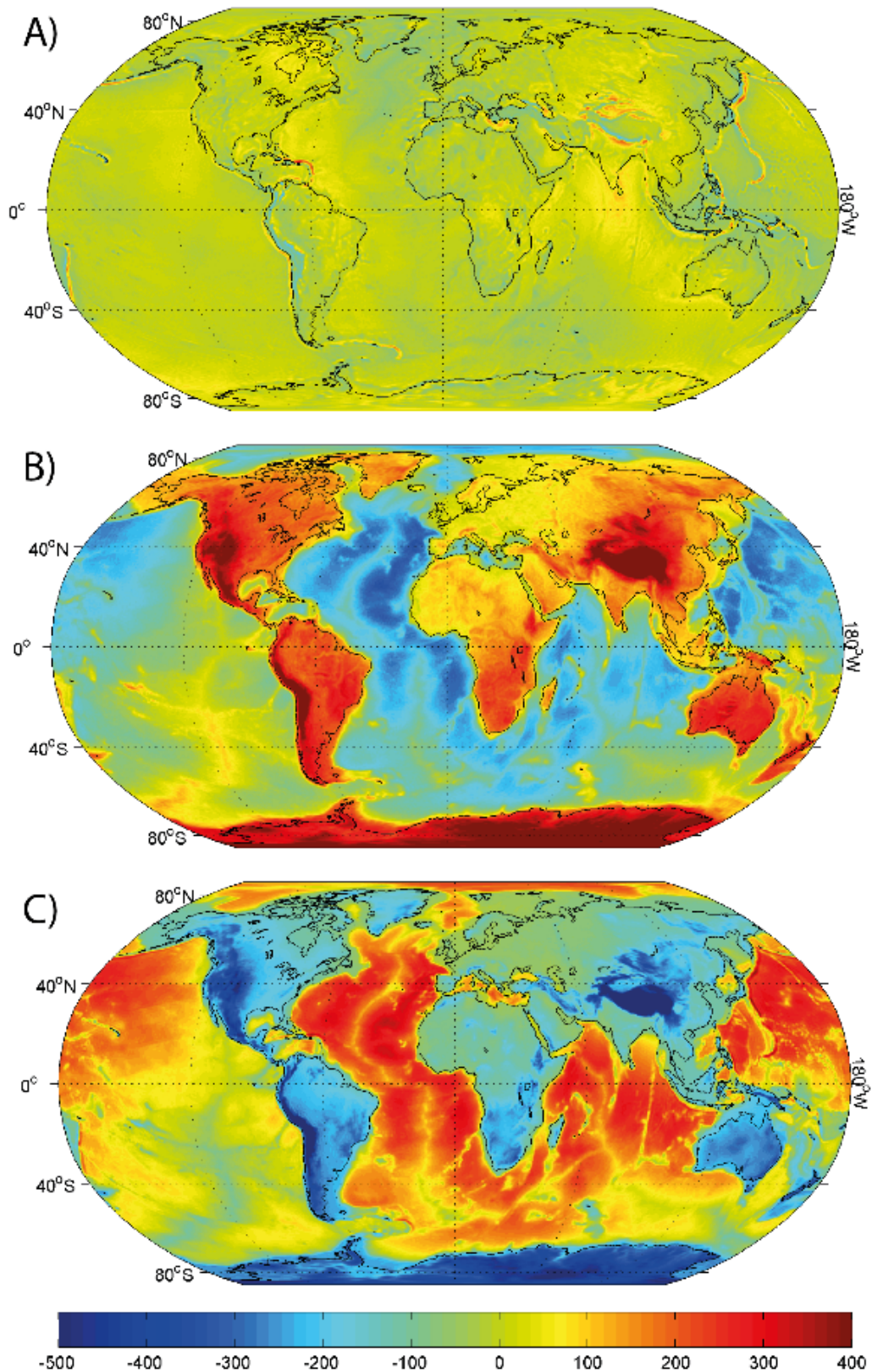
Figure 3: Global maps of gravity disturbances from a) the ESA GOCE gravity model GO_CONS_GCF_TIM5, b) the topographic potential model dV_ELL_RET2014 and c) derived Bouguer gravity anomalies (c=a - b) at an evaluation height of 10 km; models are truncated at degree 250 (units are mGal; Robinson projection).

4.3 Global Bouguer anomaly map

Following the description in section 3.4 a global Bouguer anomaly map (Fig. 3C) may be retrieved by subtracting a grid of forward modelled (topography-implied) gravity (Fig. 3B: dV_ELL_RET2014) from a grid of GOCE gravity disturbances (Fig. 3A: TIM5). and Alternatively, a difference of their potential coefficients and subsequent SHS leads to a similar result. As degree of truncation for the synthesis degree 250 has been chosen, because the signal-to-noise (SNR) ratio of an unconstrained SGG (Satellite Gravity Gradiometry)-only solution (of the time-wise method) was found to become 1 at degree 254 [17]. Beyond this degree, the error is thus expected to supersede the actual gravity signal. Because the topographic masses are treated as uncompensated, the topographic potential (Fig. 3B) shows much larger gravity signal amplitudes than the GOCE-observed field (see also Tab. 2).

Model / gravity type	Min	Max	RMS
		[mGal]	
GO_CONS_GCF_TIM5	-363	305	30
dV_ELL_RET2014	-787	396	195
Bouger gravity anomalies	-352	699	196

Table 2: Maximum and minimum gravity in a) observed gravity, b) forward modelled gravity and c) Bouguer gravity; models were evaluated at 10km height and truncated at degree 250.

5. CONCLUSION

GOCE's gravity as extracted from ESA's official GOCE gravity field models and gravity from the ellipsoidal topographic potential (forward modelled from a model of the topography) may be used in common for a range of applications and for mutual validation.

It could be shown through forward modelling of the ETP by applying the *Harmonic Combination Method* to the latest rock-equivalent topography model of Curtin University, (Earth2014 RET) how GOCE gravity field models of the TIM and DIR approach can be validated. The agreement between observed gravity and predicted (topographic) gravity is quantified in terms of reduction rates and correlation coefficients. Our analysis allow to draw the following conclusion: DIR and TIM models show constant improvement over time, as they prove to reduce topography-implied gravity to higher spherical harmonic degrees with each release. Correlations and reductions of DIR5 and TIM5 are very similar below degree 250. DIR5 shows the highest reductions beyond degree 250 and no topographic-signal seems to be contained beyond degree ~ 290 (TIM5: beyond degree ~ 280). It can thus be stated that the fifth-generation GOCE models resolve the gravity field up to 70-80 km scales. Between degree 150 to 190 the 5th generation models show lower CC and RR values than some of their predecessor models.

In a reverse manner, different topographic input models and different forward modelling techniques were evaluated using the DIR5 model as a reference. Among the evaluated topographic potential models, Curtin's dV_ELL_RET2014 ETP model shows the best agreement to GOCE gravity as represented in DIR5. This outcome is owing to the use of most up-to date topographic information over Greenland and Antarctica and other regions of Earth, and the ellipsoidal modelling technique [3] applied. Our comparisons show that Curtin's dV_ELL_RET2014 ETP model offers a slightly better performance than the RWI-model by Karlsruhe Institute of Technology (which is based on older data sets). Notwithstanding, the RET-compression is theoretically less accurate than the RWI-approach, but this effect is masked, most likely by the use of better data sets in dV_ELL_RET2014.

As a last example for common application of GOCE data and topographic data, a global Bouguer gravity anomaly map was computed from the difference between the 5th generation TIM model and the ellipsoidal topographic potential model dV_ELL_RET2014. The map improves over classical planar Bouguer maps because the gravitational effect of the global topographic masses is taken into account. Second, masses are arranged on the GRS80 ellipsoid instead of some mean sphere which improves over spherical Bouguer gravity maps [6]. The resolution of the map is 80 km (degree 250) which is close to the resolution where the signal-to-noise ratio of an unconstrained GOCE SGG-only model becomes 1. The input topography model Earth2014 [4] as well as its derived topographic potential model dV_ELL_RET2014 will soon be available through Curtin University's servers: **www.ddfe.curtin.edu.au/models/Earth2014**. Additionally, dV_ELL_RET2014 will be part of the *GOCE_User_Toolbox* [20] for the computation of Bouger anomaly maps with ESA's official GOCE gravity field models, available at https://earth.esa.int/web/guest/software-tools/gut/. For an extended report of the topographic evaluation of the fifth-generation GOCE gravity fields including detailed global and regional comparison results see [21].

6. ACKNOWLEDGEMENTS

7. REFERENCES

1. ESA (1999), Gravity Field and Steady-State Ocean Circulation Mission, *European Space Agency,* ESA **SP-1233**(1).

2. Hirt C., Kuhn M., Featherstone, W., Göttl, F. (2012) Topographic/isostatic evaluation of new-generation GOCE gravity field models, *Journal of Geophysical Research – Solid Earth,* 117, B05407, DOI:. 10.1029/2011JB008878.

3. Claessens, S., Hirt, C. (2013) Ellipsoidal topographic potential – new solutions for spectral forward modelling of topography with respect to a reference ellipsoid, *Journal of Geophysical Research,* **188**(11), 5991-6002, DOI : 10.1002/2013JB010457.

4. Hirt C., Rexer M. (2015), Earth2014: 1 arc-min shape, topography, bedrock and ice-sheet models – available as gridded data and degree 10,800 spherical harmonic. Soon available via geodesy.curtin.edu.au.

5. Rexer, M., Hirt, C. (2014) Comparison of free high resolution digital elevation data sets (ASTER GDEM2, SRTM v2.1/v4.1) and validation against accurate heights from the Australian National Gravity Database, *Australian Journal of Earth Sciences,* **61**(2), 1-15, DOI: 10.1080/08120099. 2014.884983.

6. Balmino, G. and Vales, N. and Bonvalot, S. and Briais, A. (2012) Spherical harmonic modelling to ultra-high degree of Bouguer and isostatic anomalies, *Journal of Geodesy,* **86**(7), 499-520, DOI: 10.1007/s00190-011-0533-4.

7. Kuhn, M., Seitz, K. (2005) Comparison of Newton's Integral in the Space and Frequency Domain, In: *A window on the Future of Geodesy – IAG Symposia*, Sanso,F., 128, 386-391.

8. Pail, R. and Bruinsma, S., Migliaccio, F., Förste, C., Goiginger, H., Schuh, W.-D., Höck, E., Reguzzoni, M., Brockmann, J.M., Abrikosov, O., Veicherts, M., Fecher, T., Mayrhofer, R., Krasbutter, I., Sanso, F., Tscherning, C. C. (2011) First GOCE gravity field models derived by three different approaches, *Journal of Geodesy,* **85**(11),819-843,DOI: 10.1007/s00190-011-0467-x.

9. Pavlis, N.K., Holmes, S.A., Kenyon, S.C., Factor, J.K. (2012) The development and evaluation of the Earth Gravitational Model 2008 (EGM2008*), Journal of Geophysical Research,* 117, DOI: 10.1029/2011JB008916.

10. Hirt, C., Claessens, S., Fecher, T., Kuhn, M., Pail, R., Rexer, M. (2013) New ultra-high resolution picture of Earth's gravity field, *Geophysical Research Letters,* **40**(16), 4279-4283, DOI: 10.1002/grl.50838.

11. Torge,W. (2001) Geodesy, Walter-de-Gruyter, Berlin, New York.

12. Hirt, C. (2014) GOCE's view below the ice of Antarctica: Satellite gravimetry confirms improvements in Bedmap2 Bedrock knowledge, *Geophysical Research Letters,* **41**(14), 5021-5028, DOI: 10.1002/2014GL060636.

13. Bruinsma, S., Marty, J., Balmino, G., Biancale, R., Förste, C., Abrikosov, O., Neumayer, H. (2010) GOCE gravity field recovery by means of the direct numerical method, *Proceedings of the ESA living planet symposium, Lacoste-Francis, H.,* ESA SP-686, European Space Agency.

14. Migliaccio, F., Reguzzoni, M., Sanso, F., Tscherning, C., Veicherts, M. (2010), GOCE data analysis : the space-wise method approach and the first space-wise gravity field model, *Proceedings of the ESA living planet symposium, Lacoste-Francis, H.,* ESA SP-686, European Space Agency.

15. Pail, R., Goiginger, H., Mayrhofer, R., Schuh, W.D., Brockmann, J.-M., et al. (2010) GOCE gravity model derived from orbit and gradiometry data applying the time-wise method, *Proceedings of the ESA living planet symposium, Lacoste-Francis, H.,* ESA SP-686, European Space Agency.

16. Wieczorek, M., Phillips, R. (1998) Potential anomalies on a sphere: Applications to the thickness of the lunar crust, *Journal of Geophysical Research,* **103**(E1), 1715–1724, DOI:10.1029/97JE03136.

17. Brockmann, J.M.,Zehentner, N., Höck, E., Pail, R., Loth, I., Mayer-Gürr, T., Schuh, W.D. (2014) EGM_TIM_RL05: An Independent Geoid with Centimeter Accuracy Purely Based on the GOCE Mission, *Geophysical Research Letters,* DOI: 10.1002/2014GL061904.

18. Claessens, S.J. (2005), New relations among associated Legendre functions and spherical harmonics, *Journal of Geodesy,* **79**(6-7), 589 398-406, doi: 10.1007/s00190-005-0483-9.

19. Grombein, T., X. Luo, K. Seitz und B. Heck. 2014. A wavelet-based assessment of topographic-isostatic reductions for GOCE gravity gradients. *Surveys in Geophysics* **35**(4): 959-982.

20. Knudsen, P., Benveniste, J., Andersen, O., Haines, K., Snaith, H., Johannesen, J., Rio, M.H., Niemeijer, S. (2010) The GOCE User Toolbox – GUT – An ESA Effort to Facilitate the Use of GOCE Level-2 Products, *Proceedings of the EGU General Assembly, 2-7 May, Vienna,* p.9793.

21. Hirt, C., S.J. Claessens, M. Rexer (2014), Topographic evaluation of fifth-generation GOCE gravity field models - globally and regionally, Newton's Bulletin 5, Special issue on validation of GOCE gravity fields, submitted.